Supporting Information

Evaluation of Bis-Cyclometalated Alkynylgold(III) Sensitizers for Water Photoreduction to Hydrogen

EXPERIMENTAL SECTION

General Experimental. All of the synthetic reactions for the complexes were carried out under a nitrogen atmosphere using standard Schlenk techniques. The workup and purification procedures were performed in air. 2,6-bisphenylpyridine (HC^N^CH), 2,6-bis(4-*tert*-butylphenyl)pyridine (H^{t}BuC^N^C^{t}BuH), 3,6-Di-tert-butyl-9-(4-ethynylphenyl)-9H-carbazole (HC≡CC_6H_4-3,6-di-*tert*-butyl-9H-carbazole), and the chlorogold(III) precursor compounds, [Au(C^N^C)Cl], [Au(^{t}BuC^N^C^{t}Bu)Cl] were prepared following previously reported methods and gave consistent spectroscopic data, whereas the new gold(III) complexes were synthesized as described below.[1] Unless otherwise noted, all other chemical reagents were obtained commercially and used without further purification. ^{1}H NMR spectra were recorded on a Bruker AMX-500 NMR spectrometer. Elemental microanalyses for C, H and N were measured on a Perkin-Elmer 240C element analyzer. The UV-vis measurements were performed using a Varian Cary 50 UV–Vis spectrophotometer for solutions. The fluorescence emission spectra were measured with a Varian Cary Eclipse fluorescence spectrophotometer. The fluorescence emission decay time data were acquired on a Horiba Jobin-Yvon Fluorolog-3-21-TCSPC spectrometer (τ ±10%). Electrochemical properties of the complexes in solution were obtained in a three-electrode cell consisting of a glassy carbon disk (3 mm diameter disk) working electrode, an auxiliary platinum wire and an Ag/AgCl (saturated) reference electrode using a PARSTAT-2273 advanced electrochemical system.

Syntheses of Hg(C^N^CH)Cl$_2$

A mixture of 2,6-bis(phenyl)pyridine (1.60 g, 6.92 mmol) and mercury(II) acetate (4.4 g, 13.85 mmol) in absolute ethanol (40 mL) was heated under reflux for 24 h, after which a solution of lithium chloride (1.0 g, 23.7 mmol) in methanol (20 mL) was added, and the resulting mixture was heated at 60 ^{o}C for 30 min. Upon completion of reaction, distilled water (60 mL) was added into the mixture of the solution and white precipitate was generated at once. It was filtered and washed with water and ice-cold methanol. Next, the white solid was extracted with hot methanol and evaporated to dryness to give the white solid. The product was used without further purification in the next synthetic step. Yield: 0.63 g (19.5 %).

Syntheses of [Hg(^{t}BuC^N^C^{t}BuH)Cl][2]

The procedure was similar to that for Hg(C^N^CH)Cl, except 2,6-bis(4-tertbutylphenyl)pyridine (1.91 g, 5.56 mmol) was used in place of 2,6-bis(phenyl)pyridine. Yield: 0.83 g, (25.9 %).

Syntheses of Au(C^N^C)Cl[2]

A mixture of Hg(C^N^C)Cl (308 mg, 0.66 mmol) and $KAuCl_4$ (246 mg, 0.66 mmol) in acetonitrile (45 mL) was refluxed under atmosphere of nitrogen for 24 h. After cooling to room temperature, the yellow solid was filtered and air-dried. The product was directly used for the next step of the reaction without further purification. Yield: 197 mg (64.8 %).

Syntheses of Au(^{t}BuC^N^C^{t}Bu)Cl[2]

The procedure was similar to that for Au(C^N^C)Cl, except Hg(^{t}BuC^N^C^{t}BuH)Cl (600 mg, 1.04 mmol) was used in place of Hg(C^N^C)Cl. Yield: 360 mg (60.4 %).

Synthetic procedure for gold(III) complexes

Au(C^N^C)(C≡CC_6H_5) (1). This was synthesized according to a literature method. Briefly, a mixture of [Au (C^N^C)Cl] (0.20 g, 0.43 mmol) and phenylacetylene (0.1 mL) with a catalytic amount of CuI (20 mg) in dichloromethane (35 mL) and triethylamine (2 mL) was stirred at room temperature for 5 h. After the removal of solvents by rotary evaporation, the solid residue was purified by flash column chromatography on silica gel (eluent: hexane/CH_2Cl_2 (10:1 v/v) to hexane/CH_2Cl_2 (1:1 v/v)), followed by recrystallization to obtain the product as a pure pale yellow solid. Yield: 200 mg (88.5%). ^{1}H NMR (DMSO, 500 MHz): δ 8.16 (1H, t, J = 8.0), 7.98 (2H, d, J = 8.0), 7.90 (4H, t, J = 6.0), 7.54 (2H, d, J = 7.3), 7.41(4H, m), 7.33 (3H, m). Elemental analyses (%) calcd for $C_{25}H_{16}NAu$: C, 56.94; H, 3.06; N, 2.66. Found: C, 56.66; H, 3.07; N, 2.67. ESI-MS (CH_3OH): *m/z* found 1076.83 $[2\times M+Na]^+$. Calcd: *m/z* 527.37.

Au(C^N^C)(C≡CC_6H_4-3,6-di-*tert*-butyl-9H-carbazole) (2). The reaction of [Au (C^N^C)Cl] (220 mg, 0.52 mmol) with 3,6-di-tert-butyl-9-(4-ethynylphenyl)-9H-carbazole (300 mg, 0.79 mmol) following the general procedure yielded **2** as yellow solid, which was purified by column chromatography on silica (eluent: hexane/CH_2Cl_2 (2:1 v/v) to CH_2Cl_2) and further recrystallization. Yield: 316 mg (75.5%). ^{1}H NMR (DMSO, 500 MHz): δ 8.31 (2H, s), 8.20 (1H, s), 7.99 (4H, t, J = 9.2), 7.94 (2H, s), 7.80 (2H, d, J = 7.6), 7.62 (2H, d, J = 7.9), 7.52 (2H, d, J = 7.9), 7.46 (2H, s), 7.38 (4H, m), 1.44 (16H, s). Elemental analyses (%) calcd for $C_{46}H_{40}NAu$: C, 68.74; H, 5.02; N, 1.74. Found: C, 68.48; H, 5.14; N, 1.67. ESI-MS (CH_3OH): *m/z* found 827.25 $[M+Na]^+$, and 1632.08 $[2\times M+Na]^+$. Calcd: *m/z* 804.77.

Au(^{t}BuC^N^C^{t}Bu)(C≡CC_6H_5) (3). The reaction of [Au (^{t}BuC^N^C^{t}Bu)Cl] (220 mg, 0.38 mmol) with phenylacetylene (0.1 mL) following the general procedure yielded **3** as a yellow solid, which was purified by column chromatography on silica (eluent: hexane/CH_2Cl_2 (2:1 v/v)) and further recrystallization. Yield: 232 mg (95.8%). ^{1}H NMR (DMSO, 500 MHz): δ 8.10 (1H, t, J = 8.0), 8.04 (2H, d, J = 1.5), 7.86

(2H, d, J = 8.0), 7.81 (2H, d, J = 8.2), 7.49 (2H, d, J = 7.3), 7.42 (2H, t, J = 7.5), 7.35 (3H, m), 1.34 (18H, s). Elemental analyses (%) calcd for $C_{33}H_{32}NAu$: C, 61.97; H, 5.04; N, 2.19. Found: C, 61.86; H, 5.12; N, 2.26. ESI-MS (CH_3OH): *m/z* found 662.33 $[M+Na]^+$, 1301.77 $[2\times M+Na]^+$. Calcd: *m/z* 639.58.

Au(^{t}BuC^N^C^{t}Bu)(C≡CC_6H_4-3,6-di-*tert*-butyl-9H-carbazole) (4). The reaction of [Au(^{t}BuC^N^C^{t}Bu)Cl] (220 mg, 0.38 mmol) with 3,6-di-tert-butyl-9-(4-ethynylphenyl)-9H-carbazole (218 mg, 0.57 mmol) following the general procedure yielded **4** as a pale yellow solid, which was purified by column chromatography on silica (eluent: hexane/CH_2Cl_2 (2:1 v/v) and further recrystallization. Yield: 270 mg (68.7%). ^{1}H NMR (DMSO, 500 MHz): δ 8.31 (2H, s), 8.14 (1H, t, J = 8.0), 8.10 (2H, s), 7.92 (2H, d, J = 8.0), 7.85 (2H, d, J = 8.2), 7.76 (2H, d, J = 8.2), 7.68 (2H, d, J = 8.3), 7.52 (2H, d, J = 8.5), 7.39 (4H, m), 1.44 (18H, s), 1.37 (16H, s). Elemental analyses (%) calcd for $C_{54}H_{56}NAu$: C, 70.81; H, 6.16; N, 1.53. Found: C, 70.75; H, 6.19; N, 1.48. ESI-MS (CH_3OH): *m/z* found 879.58 $[M-^t$Bu+Na$]^+$. Calcd: *m/z* 916.98.

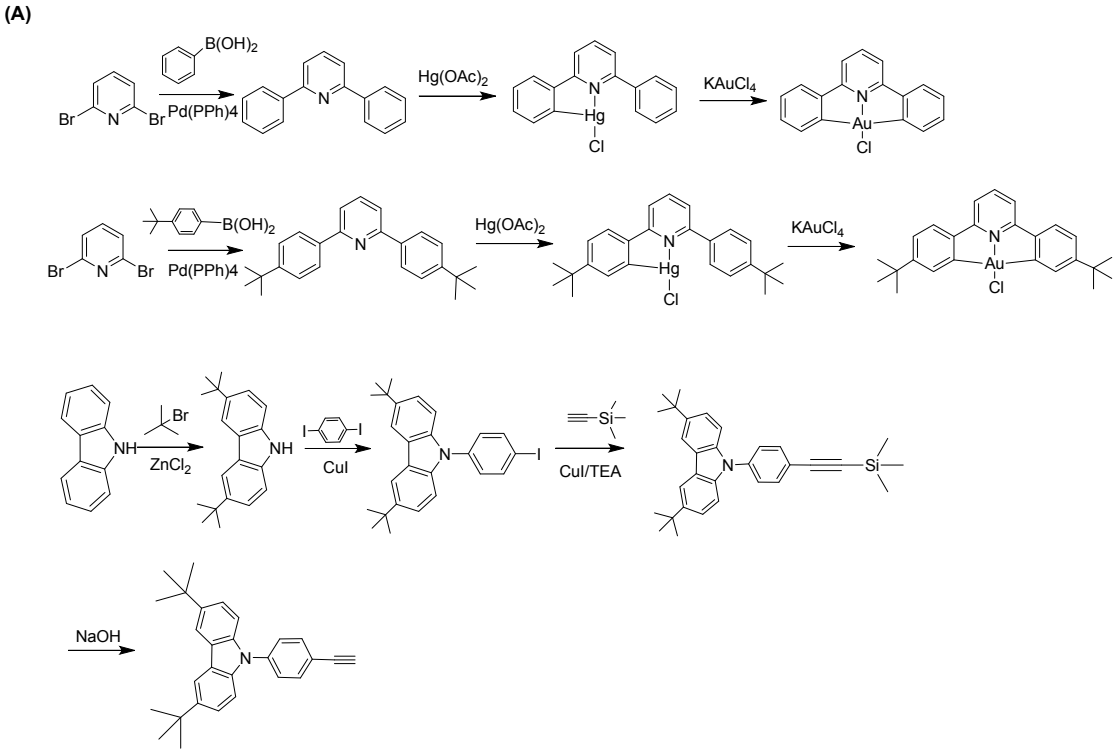

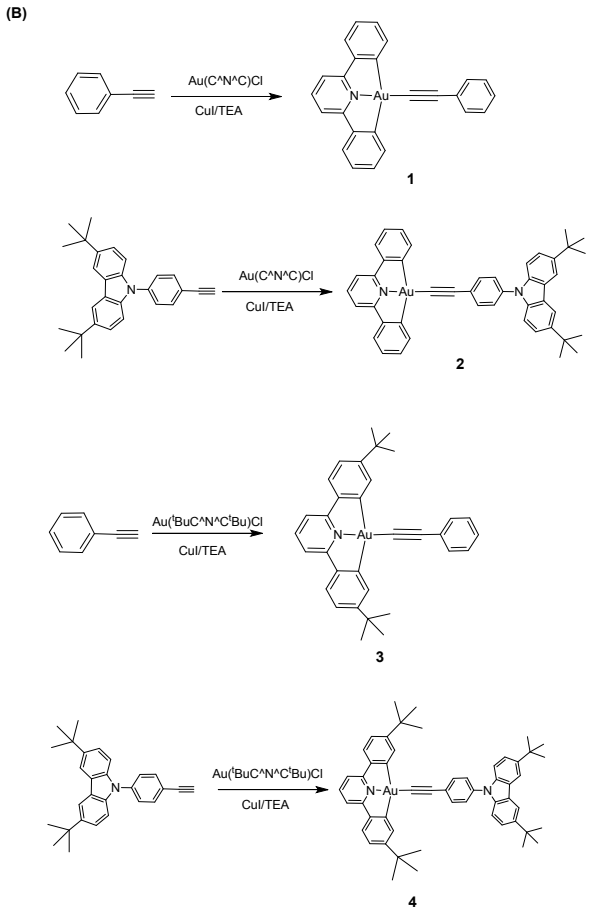

Scheme S1. Synthetic Route of **1-4**.

DFT calculations.

All calculations were performed using the Gaussian 09 program based on the density functional theory (DFT) method and time-dependent DFT (TD-DFT) calculations. The geometry optimizations of the complexes were performed for the ground states and excited state using DFT with the hybrid Perdew, Burke, and Ernzerhof functional (PBE) in conjunction with the conductor-like polarizable continuum model (CPCM) in CH_2Cl_2. For all calculations, the Stuttgart/Dresden (SDD) effective core potentials (ECP) and associated basis set were applied on the gold atom with f-type polarization functions (ζ = 1.050), whereas for all other atoms, the 6-31G (d, p) basis set was used. The numerical calculations in this paper were performed on the IBM Blade cluster system at the High Performance Computing Center (HPCC) of Nanjing University. The density functional theory calculations for complexes were performed using *Gaussian 09* package.[3]

Fluorescence Quenching. A solution of chromophore at 10 μM concentration in a CH_3CN was prepared in a quartz cuvette fitted with a septum cap. The intensity of the fluorescence was monitored by steady state fluorescence, exciting at 360 nm on a Varian Cary Eclipse fluorescence spectrophotometer. In all cases the fluorescence intensity of the chromophore solution in the absence of quencher was measured first. To each dilute chromophore solution with the same volume and concentration, incremental amounts of quencher were then added and a measurement taken after each addition.

Catalyst Poisoning Experiments

All poisoning experiments[4] were evaluated in a conventional closed circulating system with a side visible light irradiation using a 300 W xenon lamp for 6 h. A typical sample for the photocatalytic reaction studied herein contained 5 μM photosensitizer, 0.33 mM Rh(III) catalyst and 0.19 M TEOA solution in 100 mL of acetone-water (4:1, v/v) with CS_2 (0.33 mM). The pH value of the mixed solution was adjusted with concentrated hydrochloric acid as required.

Apparent quantum yield (AQY). The apparent quantum yield (AQY) can be calculated from the ratio of the number of reacted electrons ($n_{electrons}$) involved in the photocatalytic reaction to the injected photons ($n_{photons}$) as the following equations:

$$n_{photons} = \frac{P\lambda}{hc} \times t \quad (1)$$

$$AQY[\%] = \frac{\text{number of reacted electrons}}{\text{number of incident photons}} \times 100$$

$$= \frac{2 \times \text{number of evolved } H_2 \text{ molecules}}{\text{number of incident photons}} \times 100 \quad (2)$$

The $n_{electrons}$ number was double the quantity of molecular H_2 that was detected by gas chromatography. The total number of photons was calculated according to the eq (1), in which λ is the wavelength of the monochromatic light; P is the input optical power, which was measured by a Newport Model 840 optical power meter with a 1 cm^2 photodiode detector; h is Planck's constant; c is the speed of light; and t is the illumination time. The AQY was calculated according to eq (2).[5] The photocatalytic hydrogen reactions were performed for 2 h using monochromatic light irradiated at the following wavelength of 350, 380, 400, 420 and 450 nm. The light source was a Xe lamp equipped with various band-pass filters. The variation in hydrogen production was less than 10% upon repeated experiments.

References

1 R. M. Adhikari, B. K. Shah, S. S. Palayangoda, D. C. Neckers, *Langmuir*, **2009**, *25*, 2402–2406.

2 K. M.-C. Wong, L.-L. Hung, W. H. Lam, N. Zhu, V. W.-W. Yam, *J. Am. Chem. Soc.* 2007, *129*, 4350–4365.

3 M. J. Frisch, G. W. Trucks, H. B. Schlegel, G. E. Scuseria, M. A. Robb, J. R. Cheeseman, G. Scalmani, V. Barone, B. Mennucci, G. A. Petersson, H. Nakatsuji, M. Caricato, X. Li, H. P. Hratchian, A. F. Izmaylov, J. Bloino, G. Zheng, J. L. Sonnenberg, M. Hada, M. Ehara, K. Toyota, R. Fukuda, J. Hasegawa, M. Ishida, T. Nakajima, Y. Honda, O. Kitao, H. Nakai, T. Vreven, J. A. Montgomery, Jr., J. E. Peralta, F. Ogliaro, M. Bearpark, J. J. Heyd, E. Brothers, K. N. Kudin, V. N. Staroverov, R. Kobayashi, J. Normand, K.

Raghavachari, A. Rendell, J. C. Burant, S. S. Iyengar, J. Tomasi, M. Cossi, N. Rega, J. M. Millam, M. Klene, J. E. Knox, J. B. Cross, V. Bakken, C. Adamo, J. Jaramillo, R. Gomperts, R. E. Stratmann, O. Yazyev, A. J. Austin, R. Cammi, C. Pomelli, J. W. Ochterski, R. L. Martin, K. Morokuma, V. G. Zakrzewski, G. A. Voth, P. Salvador, J. J. Dannenberg, S. Dapprich, A. D. Daniels, Ö. Farkas, J. B. Foresman, J. V. Ortiz, J. Cioslowski, D. J. Fox, Gaussian, Inc., Wallingford CT, 2009.

4 B. J. Hornstein, J. D. Aiken and R. G. Finke, *Inorg. Chem.*, **2002**, *41*, 1625–1638.

5 A. Kudo, Y. Miseki, *Chem. Soc. Rev.* **2009**, *38*, 253-278.

Table S1. HOMO and LUMO Distributions of gold Complexes **1**-**4**.

Complex	HOMO-1	HOMO	LUMO
1	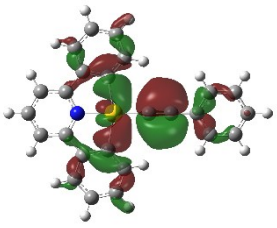 -6.51eV	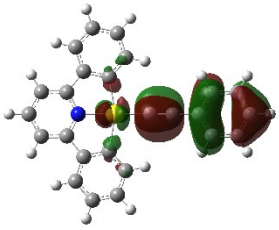 -6.30 eV	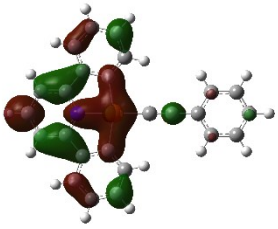 -2.17 eV
2	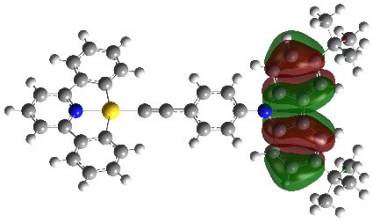 -6.14 eV	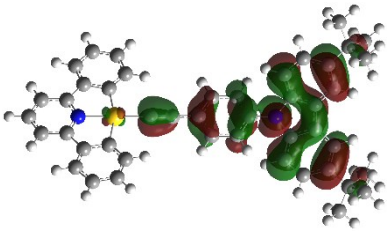 -5.53 eV	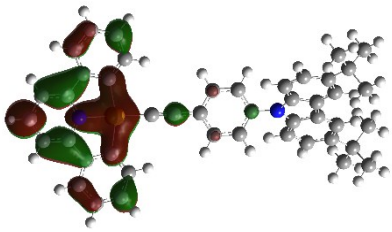 -2.18 eV
3	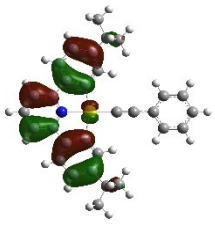 -6.34 eV	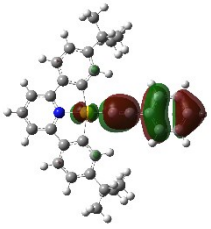 -6.30 eV	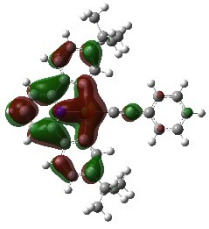 -2.09 eV
4	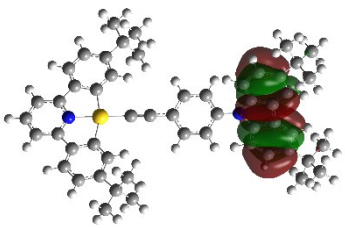 -6.14 eV	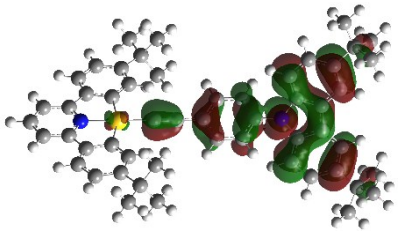 -5.53 eV	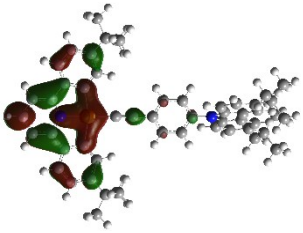 -2.10 eV

Table S2. Selected Energy Levels of studied gold(III) complexes **1–4** Calculated by TDDFT/CPCM in CH_2Cl_2[a]

Comp.	state	E_{ex} (λ)/eV (nm)	coefficient	*f*[b]	Contribution
1	S_1	3.37 (368)	0.70	0.0571	HOMO-1 → LUMO (97.35%)
	S_2	3.41 (363)	-0.39	0.0934	HOMO-2 → LUMO (30.42%)
			0.58		HOMO → LUMO (67.46%)
	T_1	2.74 (453)	0.6434	0.0000	HOMO-1 → LUMO (82.80%)
2	S_1	2.96 (419)	-0.10	0.0213	HOMO-3 → LUMO (2.12%)
			0.69		HOMO → LUMO (96.50%)
	S_2	3.37 (368)	0.70	0.0556	HOMO-2 → LUMO (97.04%)
	T_1	2.69 (460)	-0.22	0.0000	HOMO-3 → LUMO (9.85%)
			0.24		HOMO-3 → LUMO+2 (11.68%)
			0.45		HOMO → LUMO (40.77%)
			-0.30		HOMO-2 → LUMO+2 (17.81%)
3	S_1	3.31 (375)	0.70	0.1167	HOMO-1 → LUMO (96.85%)
	S_2	3.51 (354)	0.70	0.0000	HOMO-2 → LUMO (97.60%)
	T_1	2.70 (458)	0.64	0.0000	HOMO-1 → LUMO (82.79%)
4	S_1	3.03 (410)	-0.13	0.1930	HOMO-3 → LUMO (3.40%)
			0.69		HOMO → LUMO (95.04%)
	S_2	3.31 (375)	0.70	0.1160	HOMO-2 → LUMO (96.69%)
	T_1	2.70 (460)	-0.26	0.0000	HOMO-6 → LUMO (13.15%)
			0.49		HOMO-2 → LUMO+1 (47.92%)
			0.23		HOMO → LUMO (10.38%)

[a] TDDFT calculations at the optimized ground-state geometry of each compound. [b] Oscillator strengths.

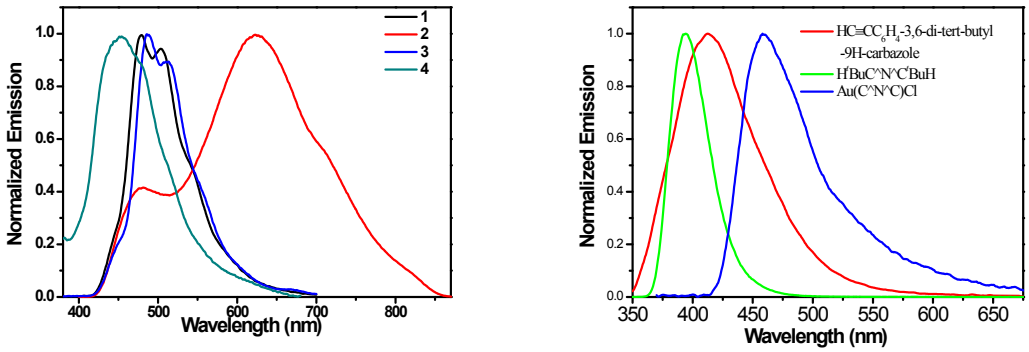

Figure S1. Emission spectra of complexes **1**–**4** (Left) and the related compounds (Right) (5×10^{-5} M, in N_2) in CH_3CN at room temperature.

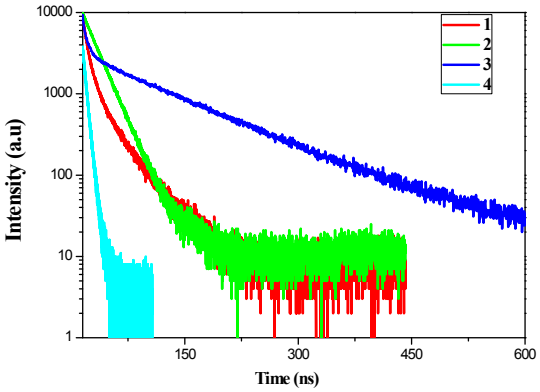

Complex	**1**	%	**2**	%	**3**	%	**4**	%
T1	10.0 ns	38.90	3.6 ns	0.55	106.9 ns	87.95	5.6 ns	29.03
T2	3.6 ns	17.25	40.4 ns	2.14	649.3 ns	4.06	14.4 ns	1.14
T3	35.1 ns	43.85	19.6 ns	97.31	5.3 ns	8.00	3.8 ns	69.82
T avg	10.1 ns		19.4 ns		42.9 ns		4.2 ns	
CHISQ	1.14		1.21		1.12		1.11	

Figure S2. Emission decay kinetics for complexes **1-4** (5×10^{-5} M) measured in nitrogen-saturated CH_3CN.

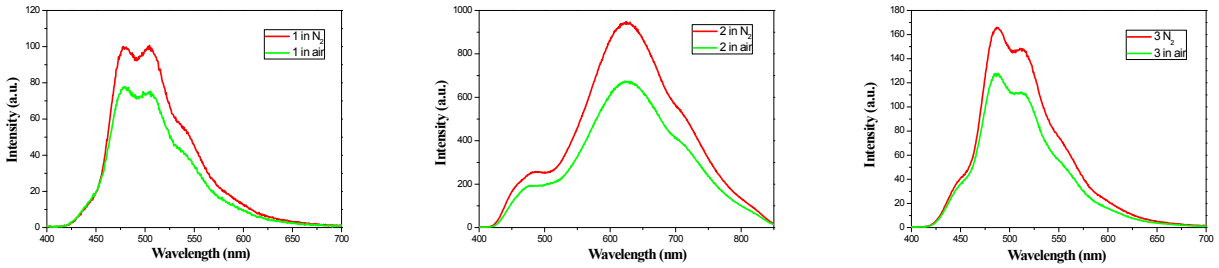

Figure S3. Photoluminescence emission spectra for complex **1-3** under a difference atmosphere of nitrogen and air.

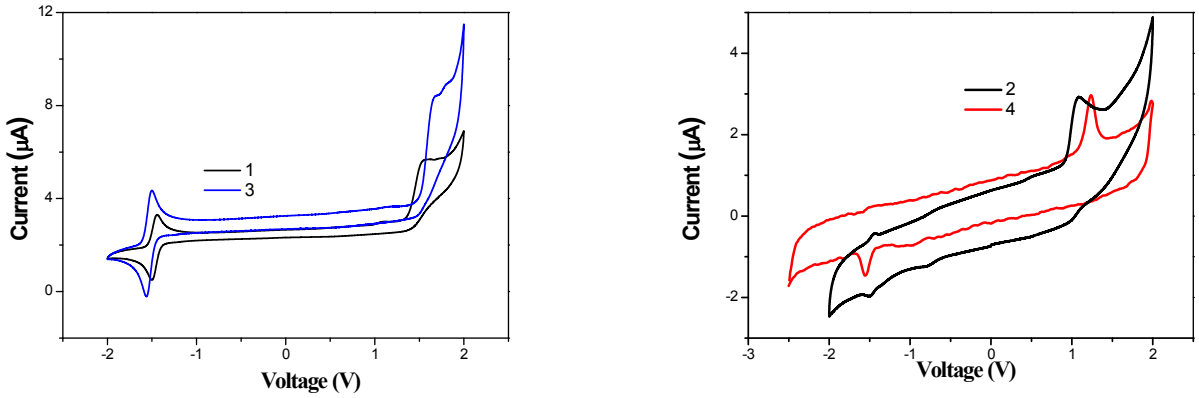

Figure S4. Cyclic voltammogram of **1-4** (ca. 10^{-3} M) in a MeCN solution at 298 K. Conditions: 0.1 M n-tetrabutylammonium hexafluorophosphate (Bu_4NPF_6) in dry acetonitrile.

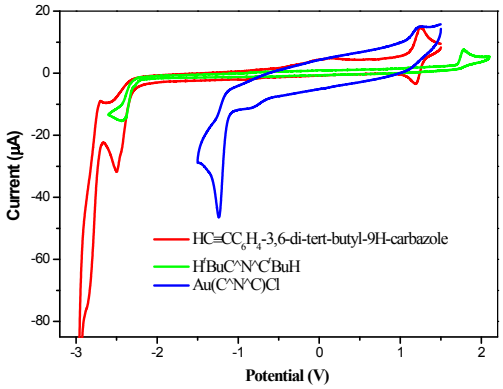

Figure S5. Cyclic voltammogram of relate compounds (ca. 10^{-3} M) in MeCN solution at 298 K. Conditions: 0.1 M n-tetrabutylammonium hexafluorophosphate (Bu_4NPF_6) in dry acetonitrile.

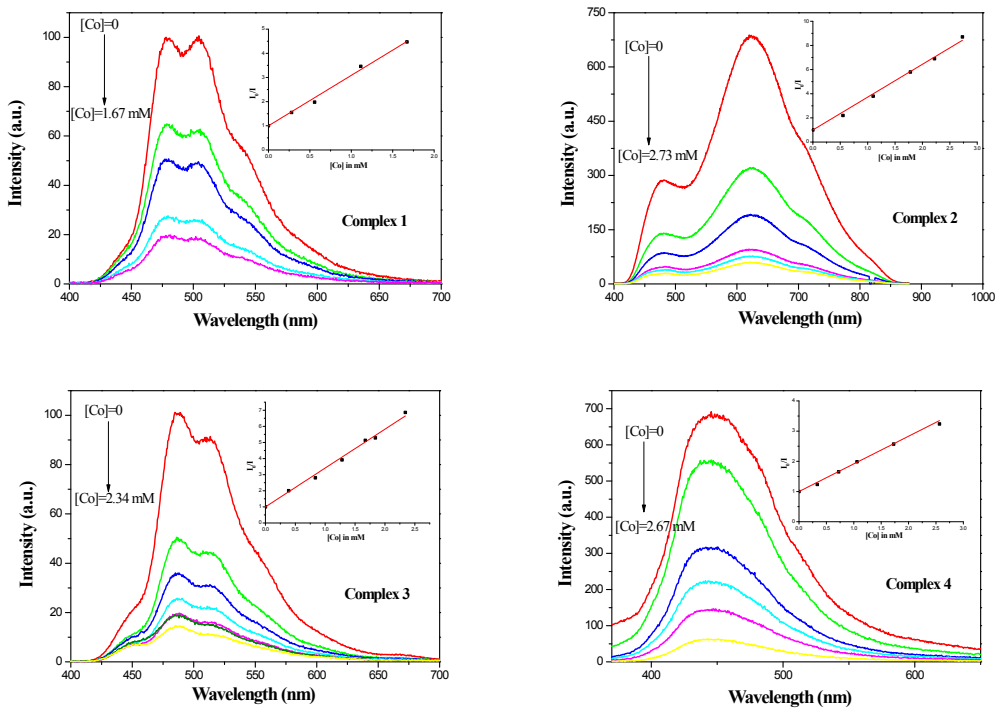

Figure S6. Emission spectra of complex **1-4** by changing the concentration of $Co(bpy)_3^{2+}$. Inset: Stern-Volmer plot for emission quenching by $[Co(bpy)_3]Cl_2$.

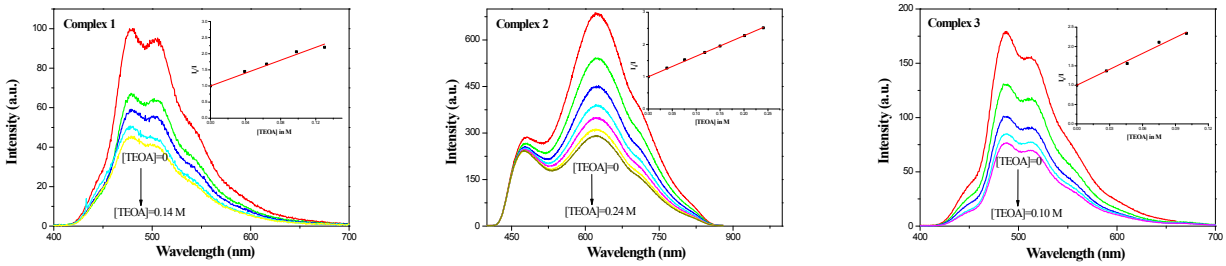

Figure S7. Emission spectra of complex **1-3** by changing the concentration of TEOA. Inset: Stern-Volmer plot for emission quenching by TEOA.

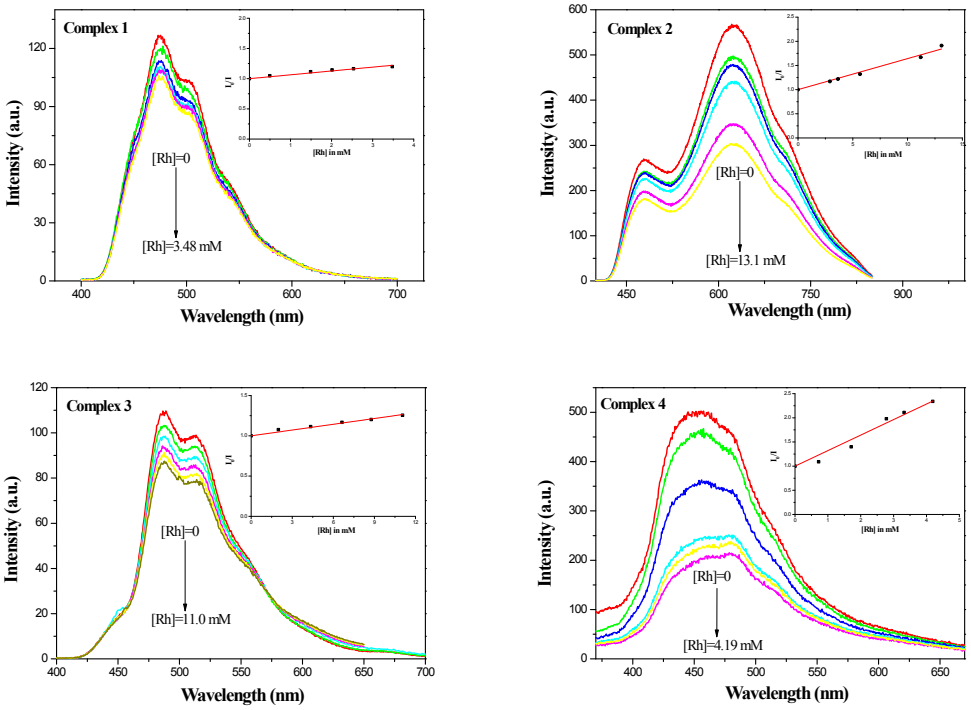

Figure S8. Emission spectra of complex **1-4** by changing the concentration of $[Rh(dtb\text{-}bpy)_3](PF_6)_3$. Inset: Stern-Volmer plot for emission quenching by $[Rh(dtb\text{-}bpy)_3](PF_6)_3$.

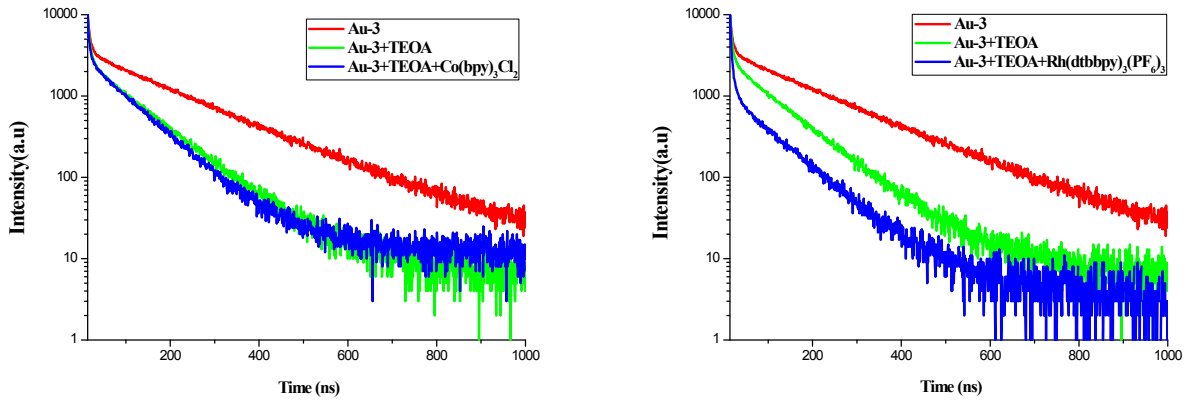

Figure S9. Emission decay kinetics for complex **3** (the concentration of complex **3** was 1×10^{-5} M) measured in nitrogen-saturated CH_3CN with the addition of TEOA (25 mM), $[Co(bpy)_3]Cl_2$ (0.3 mM) and $[Rh(dtb\text{-}bpy)_3](PF_6)_3$ (0.3 mM) at room temperature (Right).

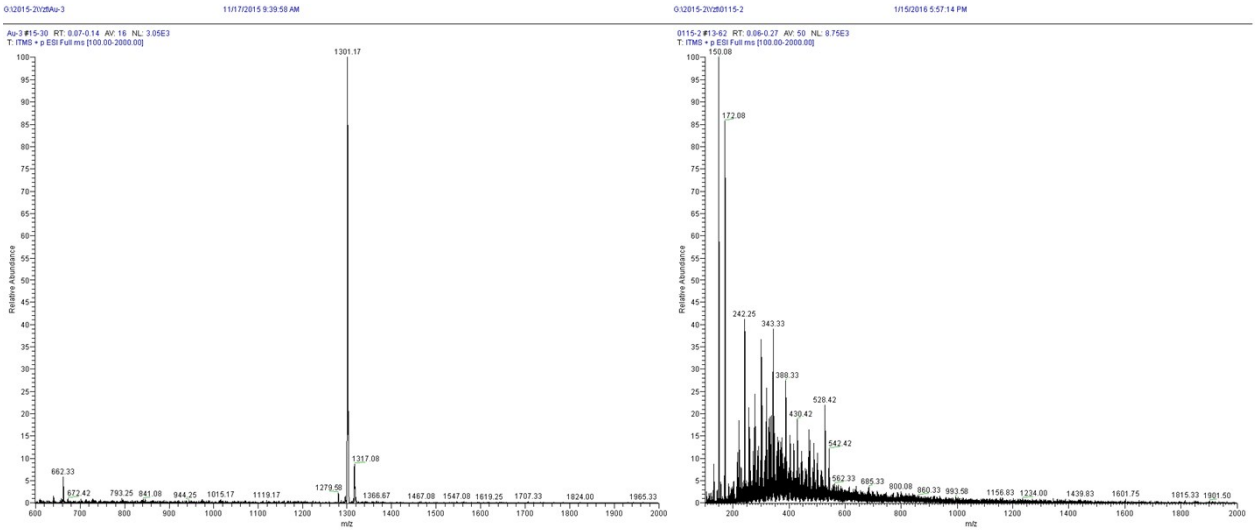

Figure S10. ESI-MS of **3** (left) and the decomposition product (right) collected from the reaction mixture of **3**-TOEA after 24 h of irradiation (Xe arc lamp; 300 W).

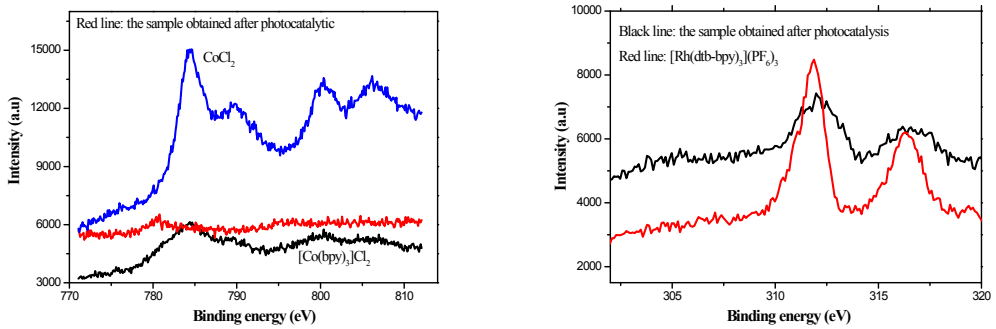

Figure S11. XPS of the catalyst (Red line) and sample (Black line) obtained after photocatalytic reaction. Conditions: **3 (**20 μM) with 0.33 mM $[Co(bpy)_3]Cl_2$ (Left) or $[Rh(dtb\text{-}bpy)_3](PF_6)_3$ (Right) and 0.19 M TEOA in acetone/water (4:1 v/v, 100 mL) upon irradiation (Xe arc lamp; 300 W). Inset in right: The photograph of dark solid particle formed after the photocatalytic experiment.

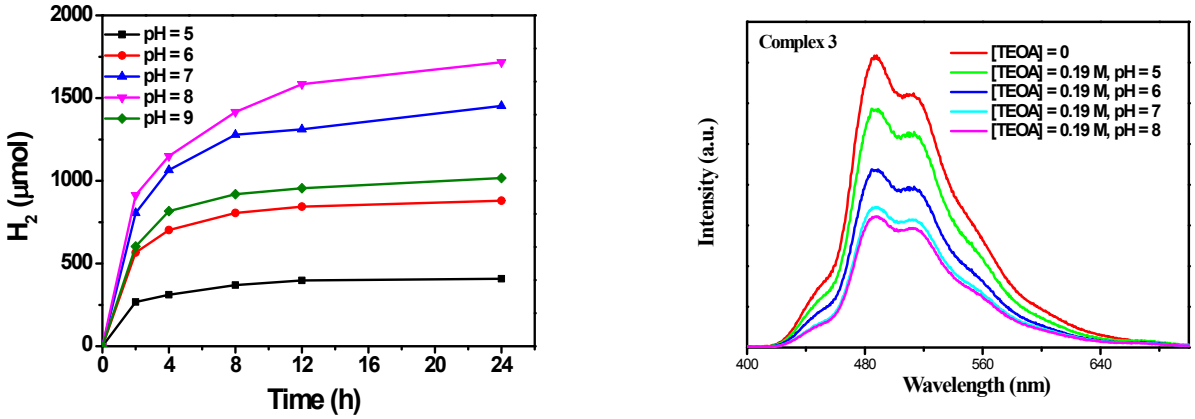

Figure S12. Effect of the pH on the photogeneration of hydrogen for **3** with $[Co(bpy)_3Cl_2]$ under light irradiation in 100 mL of 0.19 M TEOA aqueous solution (Left). Emission change of complex **3** in CH_3CN solution containing 0.19 M TEOA at the various pH (5.0, 6.0, 7.0 and 8.0) (Right).

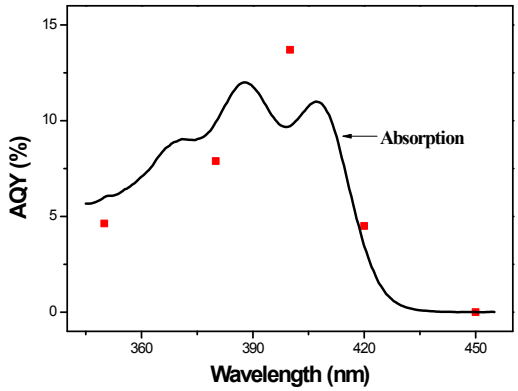

Figure S13. The quantum yield (QY) of hydrogen production of **3** *versus* the wavelength of the incident light (upon irradiation of 2 h, selected wavelengths: 350, 380, 400, 420 and 450 nm) compared with the Electronic absorption spectra.

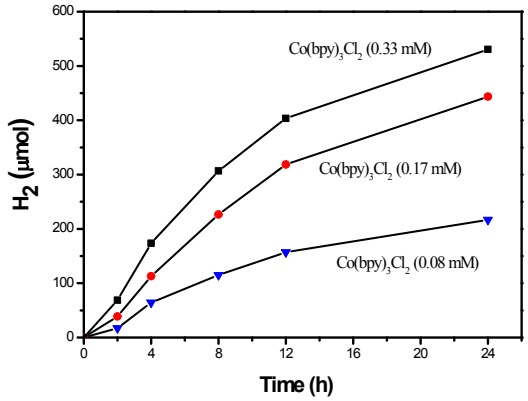

Figure S14. Effect of the concentration of $[Co(bpy)_3Cl_2]$ on the photogeneration of hydrogen for **3** under light irradiation ($\lambda > 420$ nm) in 100 mL of 0.19 M TEOA aqueous solution.

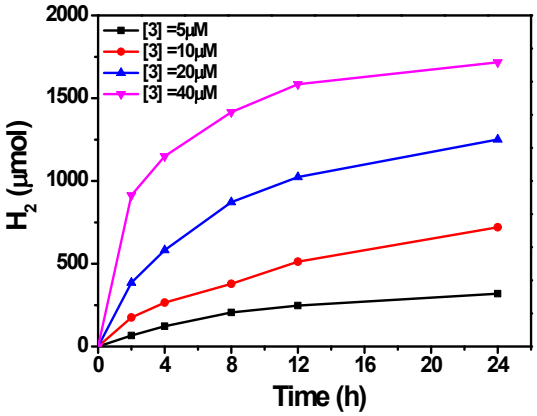

Figure S15. Photoinduced hydrogen evolution of various concentrations of **3** with $[Co(bpy)_3Cl_2]$ at pH 8.0.

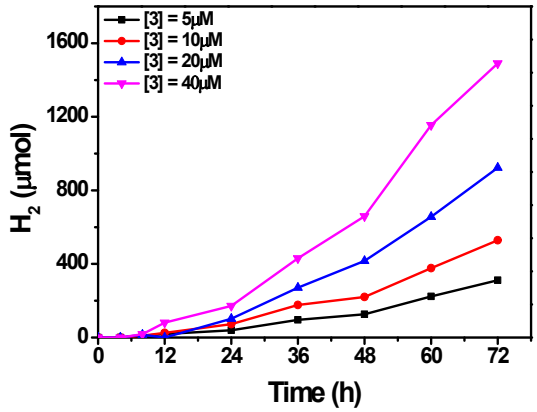

Figure S16. Photoinduced hydrogen evolution of various concentrations of **3** with $[Rh(dtb\text{-}bpy)_3](PF_6)_3$ at pH 7.0.

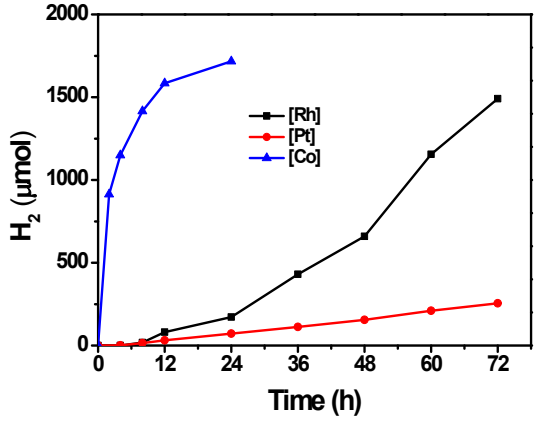

Figure S17. Photocatalytic H_2-producing activity of **3** using different catalysts.

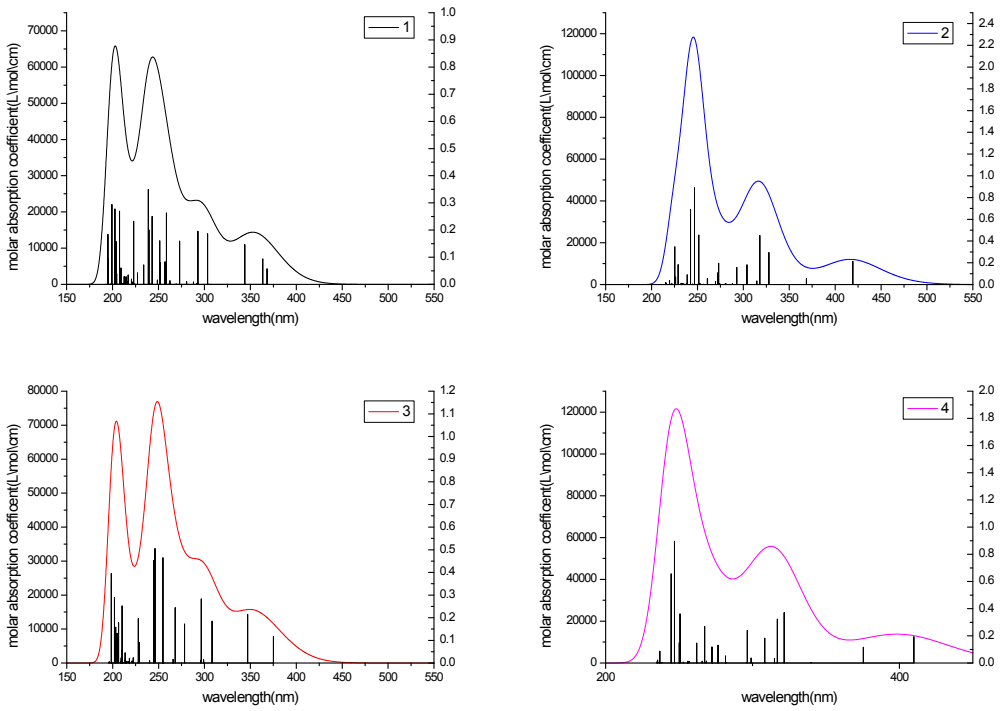

Figure S18. The ultraviolet absorption spectrum of complexes **1-4** with FWHM of 0.5eV calculated at the PBE1PBE level of theory with 6-31G (d, p) and SDD (with f-type polarization functions) basis sets.

The calculated result of TDDFT for **1-4**:

****

(Assignment; H = HOMO, L = LUMO, L+1 = LUMO+1, etc.)

Compound **1**

nstates	nm	eV	f	transition	Coeff.	Contri.
1	367.92	3.3698	0.0571	95(H-1) →97(L)	0.6977	97.3515%
2	363.19	3.4137	0.0934	94(H-2) →97(L)	-0.3900	30.4200%
				96(H)→97(L)	0.5808	67.4564%
3	343.64	3.6080	0.1464	94(H-2) →97(L)	0.5777	66.7382%
				96(H)→97(L)	0.3936	30.9842%
4	304.55	4.0711	0.0008	94(H-2) →98(L+1)	-0.3220	20.7407%
				96(H)→98(L+1)	0.6190	76.6396%
5	303.33	4.0874	0.1862	92(H-4) →98(L+1)	0.1273	3.2411%
				93(H-3) →97(L)	0.6795	92.3413%
6	292.69	4.2360	0.1952	90(H-6) →97(L)	-0.2961	17.5315%
				92(H-4) →97(L)	0.4014	32.2196%
				93(H-3) →98(L+1)	0.1073	2.3022%
				95(H-1) →98(L+1)	0.4681	43.8254%
7	291.73	4.2500	0.0041	94(H-2) →98(L+1)	0.6129	75.1317%
				96(H)→98(L+1)	0.3308	21.8804%
8	287.79	4.3082	0.0088	90(H-6) →97(L)	0.1917	7.3521%
				92(H-4) →97(L)	0.5737	65.8378%
				93(H-3) →98(L+1)	-0.1299	3.3753%
				95(H-1) →98(L+1)	-0.3292	21.6732%
9	280.35	4.4225	0.0097	89(H-7) →97(L)	0.6036	72.8593%
				90(H-6) →97(L)	-0.2321	10.7759%
				94(H-2) →99(L+2)	-0.2057	8.4658%
				95(H-1) →98(L+1)	-0.1095	2.3985%
10	272.76	4.5455	0.1590	89(H-7) →97(L)	0.2294	10.5221%
				90(H-6) →97(L)	0.5149	53.0265%
				93(H-3) →98(L+1)	-0.1093	2.3897%
				95(H-1) →98(L+1)	0.3757	28.2346%
11	269.09	4.6076	0.0020	91(H-5) →97(L)	0.6869	94.3553%
				96(H)→102(L+5)	-0.1289	3.3215%
12	262.30	4.7268	0.0137	92(H-4) →98(L+1)	0.4915	48.3105%
				94(H-2) →100(L+3)	0.2501	12.5070%
				96(H)→100(L+3)	-0.4081	33.3108%
13	261.24	4.7460	0.0011	90(H-6) →97(L)	0.1964	7.7177%
				93(H-3) →98(L+1)	0.6608	87.3234%
14	258.47	4.7969	0.2626	89(H-7) →97(L)	-0.2115	8.9456%
				94(H-2) →99(L+2)	-0.3803	28.9287%
				96(H)→99(L+2)	0.5256	55.2574%
15	256.86	4.8270	0.0833	92(H-4) →98(L+1)	0.3627	26.3059%
				94(H-2) →100(L+3)	0.1758	6.1832%
				96(H)→100(L+3)	0.5622	63.2115%

S0-Tn (f=0.000)

nstates	nm	eV	transition	Coeff.	Contri.
1	452.90	2.7376	95(H-1) → 97(L)	0.6434	82.8030%
2	451.06	2.7487	92(H-4) →97(L)	0.3013	18.1563%
			95(H-1) →98(L+1)	0.5474	59.9337%
3	424.16	2.9231	96(H) → 97(L)	-0.4389	38.5179%
			96(H) →99(L+2)	0.4532	41.0871%

4	370.40	3.3473	94(H-2) →97(L)	0.6276	78.7638%
5	347.21	3.5709	94(H-2) →97(L)	0.2605	13.5679%
			96(H) →97(L)	0.4377	38.3180%
			96(H) →99(L+1)	0.2926	17.1265%

Compound **2**

nstates	nm	eV	f	transition	Coeff.	Contri.
1	418.90	2.9597	0.2132	168(H-3) →172(L)	-0.1028	2.1156%
				171(H) →172(L)	0.6946	96.5022%
2	368.42	3.3653	0.0556	169(H-2) →172(L)	0.6966	97.0392%
3	354.36	3.4988	0.0012	167(H-4) →172(L)	0.6004	72.1008%
				168(H-3) →172(L)	0.3523	24.8174%
4	344.58	3.5982	0.0019	171(H) →173(L+1)	0.7000	97.9972%
5	339.37	3.6534	0.0000	170(H-1) →172(L)	0.7042	99.1654%
6	327.58	3.7849	0.2940	167(H-4) →172(L)	-0.3501	24.5182%
				168(H-3) →172(L)	0.5862	68.7331%
				171(H) →172(L)	0.1024	2.0959%
				171(H) →174(L+2)	0.1009	2.0374%
7	317.76	3.9019	0.4496	171(H) →174(L+2)	0.6810	92.7631%
8	314.53	3.9419	0.0326	170(H-1) →180(L+8)	-0.1306	3.4092%
				171(H) →175(L+3)	0.6858	94.0671%
9	303.68	4.0828	0.1818	164(H-7) →173(L+1)	-0.1255	3.1526%
				165(H-6) →172(L)	0.6814	92.8476%
10	296.94	4.1754	0.0003	161(H-10) →173(L+1)	-0.1207	2.9161%
				167(H-4) →173(L+1)	0.5902	69.6743%
				168(H-3) →173(L+1)	0.3620	26.2102%
11	292.70	4.2358	0.1565	163(H-8) →172(L)	-0.2888	16.6857%
				164(H-7) →172(L)	0.4270	36.4658%
				169(H-2) →173(L+1)	0.4518	40.8228%
12	289.87	4.2773	0.0000	170(H-1) →173(L+1)	0.7071	99.9924%
13	288.00	4.3050	0.0077	163(H-8) →172(L)	0.2017	8.1398%
				164(H-7) →172(L)	0.5547	61.5495%
				165(H-6) →173(L+1)	0.1338	3.5783%
				169(H-2) →173(L+1)	-0.3520	24.7794%
14	281.64	4.4022	0.0038	162(H-9) →172(L)	-0.1198	2.8694%
				162(H-9) →174(L+2)	0.1414	4.0005%
				171(H) →178(L+6)	0.6710	90.0455%
15	280.11	4.4262	0.0051	167(H-4) →173(L+1)	-0.3643	26.5487%
				168(H-3) →173(L+1)	0.5920	70.0928%

S0-Tn (f=0.000)

nstates	nm	eV	transition	Coeff.	Contri.
1	460.38	2.6931	168(H-3) →172(L)	-0.2219	9.8461%
			168(H-3) →174(L+2)	0.2416	11.6760%
			171(H) →172(L)	0.4515	40.7723%
			171(H) →174(L+2)	-0.2984	17.8073%
2	453.29	2.7352	169(H-2) →172(L)	0.6425	82.5561%
3	449.47	2.7585	169(H-2) →173(L+1)	0.5234	54.7979%
4	403.81	3.0703	170(H-1) →175(L+3)	0.5409	58.5232%
5	393.78	3.1486	168(H-3) →174(L+2)	-0.2779	15.4479%
			171(H) →172(L)	0.5151	53.0553%
			171(H) →174(L+2)	0.2955	17.4688%

Compound **3**

nstates	nm	eV	f	transition	Coeff.	Contri.
1	374.90	3.3071	0.1167	127(H-1) →129(L)	0.6959	96.8470%
2	354.17	3.5007	0.0000	126(H-2) →129(L)	0.6986	97.6000%
3	346.78	3.5753	0.2145	128(H) →129(L)	0.7002	98.0672%
4	308.08	4.0244	0.1846	124(H-4) →130(L+1)	-0.1017	2.0706%
				125(H-3) →129(L)	0.6797	92.3875%
5	298.87	4.1485	0.0142	124(H-4) →129(L)	0.6681	89.2688%
				127(H-1) →130(L+1)	0.1880	7.0703%
6	298.47	4.1540	0.0002	121(H-7) →130(L+1)	-0.1176	2.7669%
				126(H-2) →130(L+1)	0.6946	96.4855%
7	296.30	4.1844	0.2830	122(H-6) →129(L)	-0.3643	26.5356%
				124(H-4) →129(L)	-0.1744	6.0796%
				125(H-3) →130(L+1)	0.1137	2.5851%
				127(H-1) →130(L+1)	0.5542	61.4342%
8	295.52	4.1955	0.0117	128(H) →130(L+1)	0.7026	98.7322%
9	279.97	4.4284	0.0000	121(H-7) →129(L)	0.6390	81.6693%
				121(H-7) →131(L+2)	-0.1127	2.5403%
				126(H-2) →131(L+2)	-0.2602	13.5377%
10	278.20	4.4567	0.1722	122(H-6) →129(L)	0.5543	61.4430%
				125(H-3) →130(L+1)	-0.1521	4.6244%
				127(H-1) →130(L+1)	0.3823	29.2261%
11	267.99	4.6265	0.2445	122(H-6) →130(L+1)	0.1068	2.2825%
				124(H-4) →130(L+1)	0.6503	84.5702%
				125(H-3) →129(L)	0.1184	2.8051%
				126(H-2) →132(L+3)	0.1942	7.5458%
12	265.69	4.6665	0.0160	122(H-6) →129(L)	0.2161	9.3433%
				125(H-3) →130(L+1)	0.6557	85.9885%
13	265.26	4.6741	0.0024	123(H-5) →129(L)	0.6776	91.8338%
				123(H-5) →131(L+2)	-0.1168	2.7303%
				128(H) →134(L+5)	-0.1572	4.9449%
14	257.54	4.8142	0.0000	121(H-7) →129(L)	0.2620	13.7267%
				121(H-7) →131(L+2)	0.1282	3.2876%
				126(H-2) →131(L+2)	0.6090	74.1859%
				127(H-1) →132(L+3)	0.1496	4.4742%
15	255.38	4.8550	0.0014	120(H-8) →132(L+3)	-0.1068	2.2825%
				128(H) →132(L+3)	0.6960	96.8721%

S0-Tn (f=0.000)

nstates	nm	eV	transition	Coeff.	Contri.
1	458.45	2.7044	127(H-1) →129(L)	0.6434	82.7927%
2	458.02	2.7070	127(H-1) →130(L+1)	0.5603	62.7939%
3	422.41	2.9352	128(H) →129(L)	-0.4176	34.8813%
			128(H) →131(L+2)	0.4754	45.2048%
4	369.00	3.3600	126(H-2) →129(L)	0.6881	94.6991%
5	343.92	3.6050	124(H-4) →129(L)	0.5341	57.0568%
			127(H-1)→130(L+1)	0.3415	23.3272%

Compound **4**

nstates	nm	eV	f	transition	Coeff.	Contri.
1	409.59	3.0270	0.1930	200(H-3) →204(L)	-0.1303	3.3956%

				203(H) →204(L)	0.6893	95.0379%
2	375.15	3.3050	0.1160	201(H-2) →204(L)	0.6953	96.6884%
3	353.51	3.5072	0.0001	199(H-4) →204(L)	0.4503	40.5558%
				200(H-3) →204(L)	0.5239	54.8880%
4	339.65	3.6504	0.0023	200(H-3) →205(L+1)	-0.1096	2.4024%
				203(H) →205(L+1)	0.6978	97.3961%
5	332.05	3.7339	0.0000	202(H-1) →204(L)	0.7037	99.0500%
6	321.27	3.8592	0.3705	199(H-4) →204(L)	0.4932	48.6512%
				200(H-3) →204(L)	-0.4101	33.6413%
				203(H) →204(L)	-0.1087	2.3618%
				203(H) →206(L+2)	-0.2324	10.7973%
7	316.68	3.9151	0.3226	199(H-4) →204(L)	0.1930	7.4521%
				200(H-3) →204(L)	-0.1518	4.6062%
				203(H) →206(L+2)	0.6484	84.0923%
8	314.67	3.9401	0.0334	202(H-1) →212(L+8)	-0.1301	3.3847%
				203(H) →207(L+3)	0.6834	93.4071%
9	308.15	4.0235	0.1819	197(H-6) →205(L+1)	0.1022	2.0902%
				198(H-5) →204(L)	0.6797	92.3930%
10	298.78	4.1497	0.0360	197(H-6) →204(L)	0.6735	90.7097%
				201(H-2) →205(L+1)	0.1618	5.2358%
11	298.15	4.1584	0.0002	193(H-10) →205(L+1)	-0.1041	2.1661%
				199(H-4) →205(L+1)	0.4433	39.3030%
				200(H-3) →205(L+1)	0.5285	55.8561%
12	296.22	4.1855	0.2396	195(H-8) →204(L)	-0.3562	25.3800%
				197(H-6) →204(L)	-0.1409	3.9711%
				198(H-5) →205(L+1)	-0.1165	2.7149%
				201(H-2) →205(L+1)	0.5643	63.6801%
13	285.82	4.3379	0.0000	202(H-1) →205(L+1)	0.7071	99.9924%
14	281.69	4.4015	0.0034	194(H-9) →204(L)	-0.1016	2.0641%
				194(H-9) →206(L+2)	0.1416	4.0073%
				203(H) →210(L+6)	0.6739	90.8175%
15	281.38	4.4063	0.0515	193(H-10) →204(L)	0.4466	39.8957%
				195(H-8) →204(L)	0.4074	33.1982%
				199(H-4) →206(L+2)	-0.1844	6.7999%
				200(H-3) →206(L+2)	-0.1529	4.6757%
				201(H-2) →205(L+1)	0.2206	9.7338%

S0-Tn (f=0.000)

nstates	nm	eV	transition	Coeff.	Contri.
1	459.54	2.6980	197(H-6) →204(L)	-0.2564	13.1472%
			201(H-2) →205(L+1)	0.4895	47.9162%
			203(H) →204(L)	0.2278	10.3822%
2	458.76	2.7026	201(H-2) →204(L)	0.6427	82.6024%
3	451.86	2.7439	200(H-3) →206(L+2)	0.2376	11.2879%
			201(H-2) →205(L+1)	-0.2809	15.7776%
			203(H) →204(L)	0.3683	27.1290%
			203(H) →206(L+2)	-0.3149	19.8337%
4	403.76	3.0707	202(H-1) →207(L+3)	0.5420	58.7420%
5	388.79	3.1890	203(H) →204(L)	0.5347	57.1915%